Giant Enhancement in Low Energy Photoemission of Ar Confined in C_{60}

Mohamed E. Madjet,[1] Himadri S. Chakraborty,[2] and Steven T. Manson[3]

[1]*Institut für Chemie (Kristallographie), Freie Universitaet, Takustrasse 6, D-14195 Berlin, Germany*
[2]*Department of Chemistry and Physics, Northwest Missouri State University, Maryville, Missouri 64468, USA*
[3]*Department Physics and Astronomy, Georgia State University, Atlanta, Georgia 30303, USA*

(Received 29 August 2007; published 11 December 2007)

Considering an Ar atom endohedrally sequestered in C_{60}, a phenomenal increase in the photoionization cross section of the confined atom through the dominant outer $3p$ channel is predicted. The effect occurs owing to a powerful dynamical coherent interchannel coupling between the atomic and the cage ionization channels which redirects the bulk of oscillator strength from the giant surface plasmon to the atomic ionization.

DOI: 10.1103/PhysRevLett.99.243003 PACS numbers: 33.80.Eh, 36.40.Cg, 61.48.+c

The study of the behavior of confined atoms is in its infancy. Confinement can be achieved by optically trapping the atom or by placing it inside a material cage. Good candidates for the latter are fullerenes whose hollow geometry offers a unique possibility to examine how an atom in a stable, neutral, or charged cage responds to an external stimulus. In recent years it has been possible to synthesize fullerene compounds endohedrally doped with a variety of atoms and molecules [1]. Since these endohedral fullerenes are essentially a new form of molecular matter, their study is of great fundamental interest. In addition, because these structures are among the simplest prototypes of a host of nanomaterials, investigation of these can provide insights that apply to systems far beyond the particular compound studied.

Technologically, endohedral fullerenes hold the promise of exciting applications. Among these is their potential to be used as seed materials in solid state quantum computations by encoding qubits in electronic spins of the encapsulated atom [2,3]. In addition, the prospect of using them as agents for improving the superconducting ability of materials is fairly bright [4]. And, the discovery of endohedral fullerenes with trapped noble gases in extraterrestrial environments [5] affirms the relevance of these materials also in astrophysics.

Understanding the influence of the confining cage on the spectroscopy of the atom inside is, therefore, a matter of significant interest. Theoretical work detecting confinement-induced oscillations in the photoionization cross section of the central atom has been reported [6]. These oscillations, being geometric in nature, can be understood from an independent particle viewpoint, which also explains oscillations in C_{60} valence emissions [7]. A number of studies have been reported that employed simple models of the C_{60} cage potential to examine the effect of the confinement oscillation on various atomic resonances [8,9]. Efforts have also been put forth to elucidate interesting effects *via* a density functional-type description of the molecular orbitals of various endohedral compounds [10]. However, a major limitation of these studies is the omission of the dynamical coupling of the electrons of the confined atom to the cage electrons, particularly to their collective motion. Calculations including a many-body description of electrons in the cage have indicated some modifications of the $4d$ giant photoresonance for Ba [11,12] and Xe [12] in C_{60}. But these $4d$ resonances occur at energies well beyond where plasmons arising from the collective motions of the cage electrons appear [13]. However, based upon a simple semiclassical model, significantly more extensive effects are recently suggested in the neighborhood of the C_{60} plasmons [14,15]. Therefore, since atomic valence electrons begin to ionize at energies where the plasmons dominate, it is of great interest to explore valence photoionization of an atom, A, confined in C_{60} ($A@C_{60}$) using a theoretical methodology that explicitly includes the coupling between atomic and cage electron dynamics. In this Letter, then, we report on a study of the valence photoionization of $Ar@C_{60}$ which reveals that the coupling produces spectacular effects, significantly larger than those envisioned by simple models [14,15].

Density functional theory is used to describe the electronic structure of the C_{60} cage. This utility of this methodology was demonstrated with the explanation of the measured oscillations in the valence photoelectron intensities of neutral C_{60} [7] and the good agreement with a recent experimental study of the surface plasmon as well as a new higher-energy plasmon resonance in the photoionization of C_{60} cations [13,16]. In the formulation for the C_{60} ground state, the four valence electrons ($2s^2 2p^2$) of each carbon atom are rendered delocalized while the core C^{4+} ions (each consisting of a carbon nucleus plus two very tightly bound $1s$ electrons) are represented by a classical spherical jellium shell (with a radius $R = 3.54$ Å and a thickness Δ), augmented by a constant potential V_0 to ensure quantitative accuracy [12]. We place Ar at the center of the sphere which is a good approximation, since

the charge transfer interaction of the closed shell atom with the cage is weak. The Kohn-Sham equations for the system of 258 electrons (18 from Ar and 240 delocalized electrons from the C_{60} cage) are then solved to obtain the ground state in the local density approximation (LDA). V_0 and Δ are determined by requiring charge neutrality and by producing a value, -7.54 eV, of the first ionization potential which is very close to the experimental value for C_{60}. The width Δ is found to be 1.5 Å.

The ground state radial potential becomes orbital specific owing to the correction to avoid self-interactions of electrons [17]. In Fig. 1 the *average* radial potential of the compound is shown, along with the occupied single-electron energy levels. Note that the harmonic oscillator nomenclature is used for the cage levels, which are classified as σ_ℓ ($n = 1$) and π_ℓ ($n = 2$), where ℓ denotes the orbital angular momentum with respect to the center. π wave functions have one radial node, while the σ wave functions are nodeless. Owing to the strong delocalization effect, the σ and π levels exhibit compact energy spacings and produce very nearly the same spectrum as the pristine (empty) C_{60}, indicating the stability of the cage's electronic structure. The atomic levels, of which the valence $3p$ (-14.9 eV) and $3s$ (-29.7 eV), are in this energy region, are also shown. The atomic wave functions are somewhat hybridized, i.e., some mixing of the atomic and cage wave functions occurs, as exhibited by the extra nodal structure in the vicinity of the cage in the radial $3p$ wave function (top panel, Fig. 1). Technically this wave function is of $4p$ character due to the mixing-induced additional node. However, the mixing is weak as is evident from the small amplitude of the structure when compared with the size of the pristine C_{60} wave functions, as seen in Fig. 1. Consequently, the $3p$ binding energy of confined Ar is reduced only by about 7% compared to free Ar.

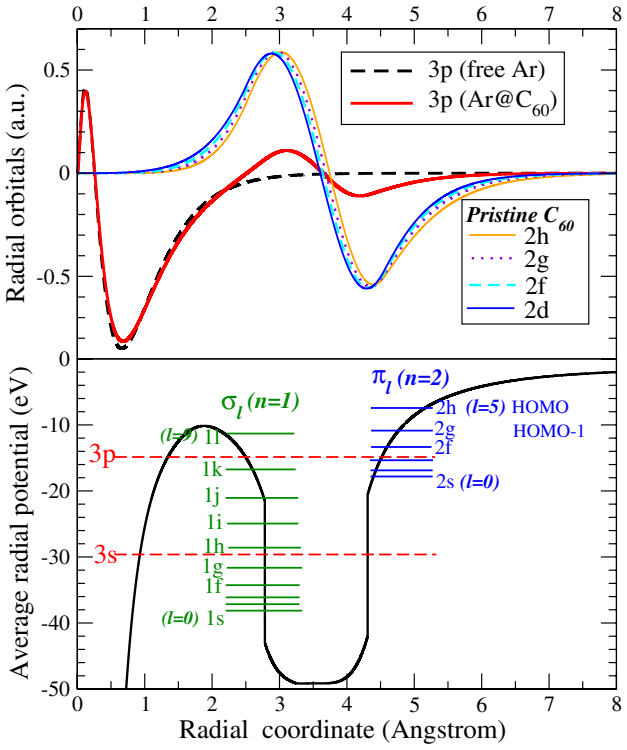

FIG. 1 (color online). Bottom panel: The average radial LDA ground state potential. All C_{60} single-electron levels and the valence $3s$, $3p$ levels of the confined Ar are shown. Top panel: Free and confined Ar $3p$ radial wave functions. The radial wave functions of some pristine C_{60} levels are also displayed.

A time-dependent LDA (TDLDA) methodology [18] is employed to calculate the dynamical response of the system to the external dipole field. The perturbation z, the dipole interaction for linearly polarized light, induces a frequency-dependent complex change in the electron density arising from dynamical electron correlations. This can be written, using the LDA susceptibility χ_0, as

$$\delta\rho(\mathbf{r};\omega) = \int \chi_0(\mathbf{r},\mathbf{r}';\omega)\delta V(\mathbf{r}';\omega)d\mathbf{r}', \tag{1}$$

in which

$$\delta V(\mathbf{r}';\omega) = z + \int \frac{\delta\rho(\mathbf{r}';\omega)}{|\mathbf{r}-\mathbf{r}'|}d\mathbf{r}' + \left[\frac{\partial V_{\mathrm{xc}}}{\partial\rho}\right]_{\rho=\rho_0}\delta\rho(\mathbf{r};\omega), \tag{2}$$

where the second and third term on the right-hand side are, respectively, the induced change of the Coulomb and the exchange-correlation potentials. Obviously, besides containing the external perturbation z, δV also includes the dynamical field produced by important electron correlations. The photoionization cross section is then calculated as the sum of independent partial cross sections $\sigma_{n\ell\to k\ell'}$, corresponding to a dipole transition $nl \to kl'$:

$$\sigma_{\mathrm{PI}}(\omega) = \sum_{n\ell}\sigma_{n\ell\to k\ell'} \sim \sum_{n\ell} 2(2\ell+1)|\langle\phi_{k\ell'}|\delta V|\phi_{n\ell}\rangle|^2. \tag{3}$$

Clearly, replacing δV in Eq. (3) by z yields the LDA cross section that entirely omits the correlation.

The weak hybridization of the Ar $3p$ wave function results in very similar $3p$ cross sections calculated in LDA for free and confined Ar, as seen in Fig. 2. The corresponding results from TDLDA, on the other hand, show huge differences between them. Just above the $3p$ ionization threshold, the TDLDA prediction for confined atom is nearly 2 orders of magnitude larger than that of its free atom counterpart. This difference, although reduced with the increase of the photon energy, remains significant up to roughly the energy where the peak of a higher-energy plasmon [13] occurs in the cross section of the pristine C_{60} (also shown in Fig. 2).

To further emphasize how huge this enhancement is, we note that the sum (integral) over the oscillator strength distribution of a system is equal to the number of electrons of that system [19]; this sum is 18 for the Ar atom. In fact, this sum rule generally works reasonably well for individual subshells [20] so that the sum for Ar $3p$ should be 6. For

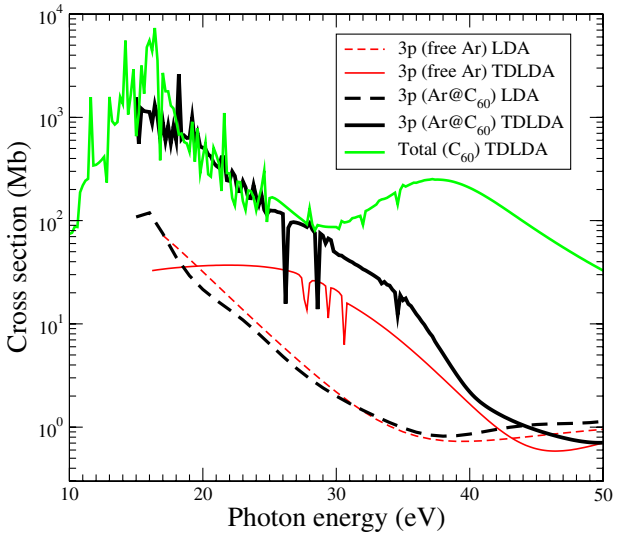

FIG. 2 (color online). Free and confined Ar $3p$ photoionization cross sections calculated both in LDA and TDLDA. The total photo cross section of the pristine C_{60} is also shown.

free Ar $3p$ from threshold to 40 eV, our calculated sum is 4.85, most of the total strength of the six electrons in the Ar $3p$ subshell. On the other hand, integrating the Ar $3p$ cross section for Ar@C_{60} over the same energy range yields a value of 60.2. This is greater than even the total number of electrons of the Ar atom, not merely the six electrons of the $3p$ subshell. Thus, it is evident that the photoionization of Ar@C_{60} $3p$ taps significantly into the oscillator strength of the C_{60} confining shell which contains 240 delocalized, relatively loosely bound electrons. In fact, the sum shows that a sizable chunk of the total oscillator strength of these 240 electrons is transferred to the $3p$ ionization channel of the confined Ar atom. We emphasize that this transfer of oscillator strength to the atom is completely different than the confinement resonances which redistribute oscillator strength only within the atom.

To understand this phenomenology, it is necessary to scrutinize the dipole matrix element responsible for the Ar@C_{60} $3p$ photoionization process, which has a dynamical dependence only on the initial and final states of Ar@C_{60}. The initial state wave function for the $3p$ electron, studied above, was found, under confinement, to remain localized on the Ar nucleus. A small amount of hybridization with the delocalized orbitals of the C_{60}, as seen in Fig. 1, is certainly not enough to account for the dramatic increase of the Ar $3p$ photoionization cross section. Thus, the increase *must* be due to alteration of the final (continuum) state wave function, i.e., interchannel coupling with the C_{60} photoionization channels.

Specifically, using the Fano formalism [21] perturbatively to characterize the effects of interchannel coupling upon the final state wave function, each of the perturbed dipole matrix elements for the Ar@C_{60} $3p$ photoionizing transitions, $M_{3p}(E)$, is given by

$$M_{3p}(E) = D_{3p}(E) + \sum_{n\ell} \int dE' \frac{\langle \psi_{n\ell}(E') | \frac{1}{|\mathbf{r}_{3p} - \mathbf{r}_{n\ell}|} | \psi_{3p}(E) \rangle}{E - E'} D_{n\ell}(E'), \quad (4)$$

where D_{3p} is the unperturbed (LDA) $3p$ matrix element, $\psi_{3p}(E)$ and $\psi_{n\ell}(E)$ are the unperturbed final continuum state wave functions of Ar@C_{60} $3p$ and $n\ell$ photoionization channels, respectively, and the sum is over all of the photoionization channels of the delocalized electrons of the C_{60} shell. The matrix element within the integral of Eq. (4) is known as the interchannel coupling matrix element; the fact that the localized $3p$ initial state wave function of the confined Ar atom overlaps somewhat with various of the C_{60} orbitals, as seen in Fig. 1, ensures that these interchannel coupling matrix elements will be of significant value. And, since the existence of the low-energy plasmon in C_{60} shows that the various dipole matrix elements for the shell electrons are "in phase" in the energy region of the plasmon, it follows that the various terms in the sum in Eq. (4) will also be "in phase," adding up coherently, leading to the dramatic enhancement seen. Indeed, since the enhancement of the $3p$ cross section of confined Ar is so great, it is clear that the second term, the perturbation correction on the right-hand side of Eq. (4), dominates overwhelmingly; the unperturbed (LDA) matrix element, D_{3p}, is largely irrelevant. In other words, this analysis shows that the Ar@C_{60} $3p$ photoionization is determined almost entirely by the interchannel coupling with the photoionization channels of the C_{60} cage orbitals in the region of the giant plasmon excitation, the 20 eV region.

It is of interest as to how these results compare with the semiclassical model [14,15]. To that end the ratio of $3p$ cross section for Ar@C_{60} and free Ar in TDLDA is shown in Fig. 3, along with the semiclassical result using the position ($\omega_1 = 16.5$ eV) and width ($\Gamma_1 = 3.5$ eV) of the C_{60} plasmon determined in our calculation. The free Ar $3p$ channel opens only at 16.1 eV. But since its cross section is smooth near threshold (Fig. 2), it can be extrapolated below threshold to roughly estimate the ratio at the threshold (14.9 eV) of the confined $3p$ result. This is also shown in Fig. 3. It is evident that the semiclassical result is qualitatively correct, but smaller in overall magnitude (note that the vertical scale of Fig. 3 is logarithmic). Also note that while the semiclassical result is universal, i.e., free of the particular choice of atom, the full calculation indicates a 1.25 eV redshift of the plasmon in Ar@C_{60} as compared to pristine C_{60}. However, it is quite remarkable that so simple a model should do as well as it does. The semiclassical model involves the notion of dynamic screening, that the C_{60} shell induces an energy-dependent screening (or enhancement) of the field associated with an incoming electromagnetic wave. But, although the semiclassical model agrees qualitatively with the full calculation, this idea of screening cannot be correct because di-

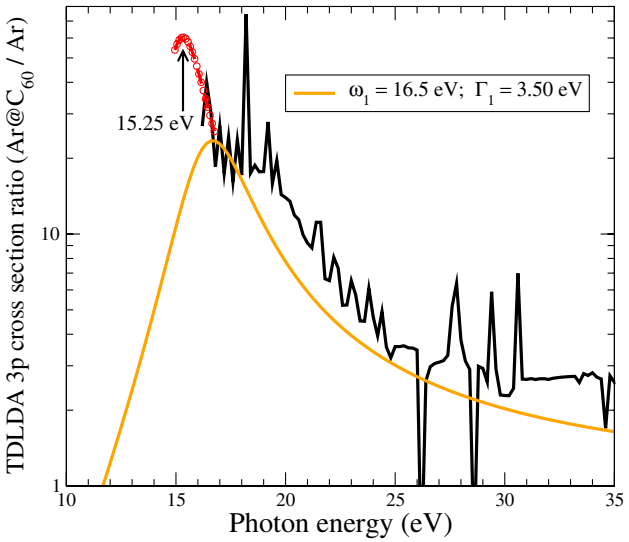

FIG. 3 (color online). Ratio of the $3p$ photionization cross sections of $Ar@C_{60}$ and free Ar and the predictions of the semiclassical model [14,15]. The extrapolation until the ratio peak (15.25 eV) is indicated (see the text).

minishing or enhancing the incoming field in an energy-dependent manner can only redistribute the oscillator strength of the confined atom. This, as we have shown, is not what happens—the oscillator strength is greatly enhanced. It would be correct to term it a dynamic coupling effect.

But owing to the sum rule, the total oscillator strength of $Ar@C_{60}$ *must* be preserved. Thus, as a consequence of the increase of the atomic cross section, the contribution of the cage to the surface plasmon is diminished to preserve the sum rule (not shown). The intensity of the depleted peak arising from the collective motion of cage electrons is reduced by 25% compared to the pristine C_{60} surface plasmon. But their widths remain roughly the same.

Note that the TDLDA calculation in the jellium frame predicts the surface plasmon redshifted about 3.5 eV from the measured position of 20 eV. However, this limitation should not affect the dramatic increase of the $Ar@C_{60}$ $3p$ photoionization cross section qualitatively, since the mechanism of the coherent interchannel coupling of the atomic with the cage ionization channels will still fundamentally hold.

In conclusion, in photoionizing $Ar@C_{60}$, it has been found that the total oscillator strength available to the system significantly redistributes between the ionization channels of the atom and the confining cage over the plasmon-active energy region owing to strong coherent coupling between these channels. This is the first prediction from a theoretical approach that treats both atomic electrons and C_{60} delocalized electrons on an equal footing. These findings illustrate a profound influence of the confining wall on the photoresponse of the confined atom that can be detected experimentally. Finally, this coherent interchannel coupling effect should be a general feature of the photoionization of atoms or molecules caged in C_{60}, or any other fullerene or fullerenelike cage, in the region of the giant plasmon resonance.

This work is supported partly by the NSF and the DOE, Basic Energy Sciences, Applied Research Grant from Northwest Missouri State University. M. E. M. and H. S. C. acknowledge the Max Planck Institute for the Physics of Complex Systems, Dresden, where most of the calculations was performed. We also thank Jan-Michael Rost for his encouragement and for valuable discussions.

[1] L. Dunsch and S. Yang, Electrochem. Soc. Interface **15**, 34 (2006).
[2] C. Ju, D. Suter, and J. Du, Phys. Rev. A **75**, 012318 (2007).
[3] W. Harneit, Phys. Rev. A **65**, 032322 (2002).
[4] A. Takeda, Y. Yokoyama, S. Ito, T. Miyazaki, H. Shimotani, K. Yakigaya, T. Kakiuchi, H. Sawa, H. Takagi, K. Kitazawa, and N. Dragoe, Chem. Commun. (Cambridge) 8 (**2006**) 912.
[5] L. Becker, R. J. Poreda, and T. E. Bunch, Proc. Natl. Acad. Sci. U.S.A. **97**, 2979 (2000).
[6] J.-P. Connerade, V. K. Dolmatov, and S. T. Manson, J. Phys. B **33**, 2279 (2000).
[7] A. Rüdel, R. Hentges, H. S. Chakraborty, M. E. Madjet, and J. M. Rost, Phys. Rev. Lett. **89**, 125503 (2002).
[8] M. Ya. Amusia, A. S. Baltenkov, L. V. Chenysheva, Z. Felfli, and A. Z. Msezane, J. Phys. B **38**, L169 (2005).
[9] A. Lyras and H. Bachau, J. Phys. B **38**, 1119 (2005).
[10] M. Stener, G. Fronzoni, D. Toffoli, P. Colavita, S. Furlan, and P. Decleva, J. Phys. B **35**, 1421 (2002).
[11] G. Wendin and B. Wästberg, Phys. Rev. B **48**, 14 764 (1993).
[12] M. J. Puska and R. M. Nieminen, Phys. Rev. A **47**, 1181 (1993).
[13] S. W. J. Scully, E. D. Emmons, M. F. Gharaibeh, R. A. Phaneuf, A. L. D. Kilcoyne, A. S. Schlachter, S. Schippers, A. Müller, H. S. Chakraborty, M. E. Madjet, and J. M. Rost, Phys. Rev. Lett. **94**, 065503 (2005).
[14] J.-P. Connerade and A. V. Solov'yov, J. Phys. B **38**, 807 (2005).
[15] S. Lo, A. V. Korol, and A. V. Solov'yov, J. Phys. B (to be published); (private communication).
[16] S. W. J. Scully, E. D. Emmons, M. F. Gharaibeh, R. A. Phaneuf, A. L. D. Kilcoyne, A. S. Schlachter, S. Schippers, A. Müller, H. S. Chakraborty, M. E. Madjet, and J. M. Rost, Phys. Rev. Lett. **98**, 179602 (2007).
[17] M. E. Madjet, H. S. Chakraborty, and J. M. Rost, J. Phys. B **34**, L345 (2001).
[18] P.-A. Hervieux, M. E. Madjet, and H. Benali, Phys. Rev. A **65**, 023202 (2002).
[19] H. A. Bethe and E. E. Salpeter, *Quantum Mechanics of One- and Two-Electron Atoms* (Springer-Verlag, Berlin, 1957), p. 255.
[20] A. F. Starace, in *Handbuch der Physik*, edited by W. Mehlhorn (Springer, Berlin, 1982), Vol. 31, pp. 1–121.
[21] U. Fano, Phys. Rev. **124**, 1866 (1961).